Research Article | Vol. 7, No. 10 | 1 Oct 2016 | BIOMEDICAL OPTICS EXPRESS 3927

Biomedical Optics EXPRESS

Quantitative chemical imaging with background-free multiplex coherent anti-Stokes Raman scattering by dual-soliton Stokes pulses

KUN CHEN,[1] TAO WU,[1] HAOYUN WEI,[1,2] TIAN ZHOU,[1] AND YAN LI[1,*]

[1]*Key Lab of Precision Measurement Technology & Instrument, Department of Precision Instrument, Tsinghua University, Beijing 100084, China*
[2]*luckiwei@mail.tsinghua.edu.cn*
[*]*liyan@mail.tsinghua.edu.cn*

Abstract: Coherent anti-Stokes Raman microscopy (CARS) is a quantitative, chemically specific, and label-free optical imaging technique for studying inhomogeneous systems. However, the complicating influence of the nonresonant response on the CARS signal severely limits its sensitivity and specificity and especially limits the extent to which CARS microscopy has been used as a fully quantitative imaging technique. On the basis of spectral focusing mechanism, we establish a dual-soliton Stokes based CARS microspectroscopy and microscopy scheme capable of quantifying the spatial information of densities and chemical composition within inhomogeneous samples, using a single fiber laser. Dual-soliton Stokes scheme not only removes the nonresonant background but also allows robust acquisition of multiple characteristic vibrational frequencies. This all-fiber based laser source can cover the entire fingerprint (800-2200 cm^{-1}) region with a spectral resolution of 15 cm^{-1}. We demonstrate that quantitative degree determination of lipid-chain unsaturation in the fatty acids mixture can be achieved by the characterization of C = C stretching and CH_2 deformation vibrations. For microscopy purposes, we show that the spatially inhomogeneous distribution of lipid droplets can be further quantitatively visualized using this quantified degree of lipid unsaturation in the acyl chain for contrast in the hyperspectral CARS images. The combination of compact excitation source and background-free capability to facilitate extraction of quantitative composition information with multiplex spectral peaks will enable wider applications of quantitative chemical imaging in studying biological and material systems.

OCIS codes: (180.5655) Raman microscopy; (180.4315) Nonlinear microscopy; (300.6230) Spectroscopy, coherent anti-Stokes Raman scattering.

References and links

1. Z. Huang, A. McWilliams, H. Lui, D. I. McLean, S. Lam, and H. Zeng, "Near-infrared Raman spectroscopy for optical diagnosis of lung cancer," Int. J. Cancer **107**(6), 1047–1052 (2003).
2. L. Bokobza and J. Zhang, "Raman spectroscopic characterization of multiwall carbon nanotubes and of composites," Express Polym. Lett. **6**(7), 601–608 (2012).
3. L. M. Almond, J. Hutchings, N. Shepherd, H. Barr, N. Stone, and C. Kendall, "Raman spectroscopy: a potential tool for early objective diagnosis of neoplasia in the oesophagus," J. Biophotonics **4**(10), 685–695 (2011).
4. T. Meyer, N. Bergner, C. Bielecki, C. Krafft, D. Akimov, B. F. Romeike, R. Reichart, R. Kalff, B. Dietzek, and J. Popp, "Nonlinear microscopy, infrared, and Raman microspectroscopy for brain tumor analysis," J. Biomed. Opt. **16**(2), 021113 (2011).
5. A. Zumbusch, G. R. Holtom, and X. S. Xie, "Three-dimensional vibrational imaging by coherent anti-Stokes Raman scattering," Phys. Rev. Lett. **82**(20), 4142–4145 (1999).
6. C. W. Freudiger, W. Min, B. G. Saar, S. Lu, G. R. Holtom, C. He, J. C. Tsai, J. X. Kang, and X. S. Xie, "Label-free biomedical imaging with high sensitivity by stimulated Raman scattering microscopy," Science **322**(5909), 1857–1861 (2008).
7. C. L. Evans, E. O. Potma, M. Puoris'haag, D. Côté, C. P. Lin, and X. S. Xie, "Chemical imaging of tissue in vivo with video-rate coherent anti-Stokes Raman scattering microscopy," Proc. Natl. Acad. Sci. U.S.A. **102**(46), 16807–16812 (2005).

#269824 http://dx.doi.org/10.1364/BOE.7.003927
Journal © 2016 Received 5 Jul 2016; revised 31 Aug 2016; accepted 31 Aug 2016; published 9 Sep 2016

Biomedical Optics EXPRESS

8. B. G. Saar, C. W. Freudiger, J. Reichman, C. M. Stanley, G. R. Holtom, and X. S. Xie, "Video-rate molecular imaging in vivo with stimulated Raman scattering," Science **330**(6009), 1368–1370 (2010).
9. C. H. Camp, Jr., Y. J. Lee, J. M. Heddleston, C. M. Hartshorn, A. R. Hight Walker, J. N. Rich, J. D. Lathia, and M. T. Cicerone, "High-speed coherent Raman fingerprint imaging of biological tissues," Nat. Photonics **8**(8), 627–634 (2014).
10. D. Fu, G. Holtom, C. Freudiger, X. Zhang, and X. S. Xie, "Hyperspectral imaging with stimulated Raman scattering by chirped femtosecond lasers," J. Phys. Chem. B **117**(16), 4634–4640 (2013).
11. T. Hellerer, A. M. K. Enejder, and A. Zumbusch, "Spectral focusing: High spectral resolution spectroscopy with broad-bandwidth laser pulses," Appl. Phys. Lett. **85**(1), 25–27 (2004).
12. D. Oron, N. Dudovich, and Y. Silberberg, "Femtosecond phase-and-polarization control for background-free coherent anti-Stokes Raman spectroscopy," Phys. Rev. Lett. **90**(21), 213902 (2003).
13. R. Selm, M. Winterhalder, A. Zumbusch, G. Krauss, T. Hanke, A. Sell, and A. Leitenstorfer, "Ultrabroadband background-free coherent anti-Stokes Raman scattering microscopy based on a compact Er:fiber laser system," Opt. Lett. **35**(19), 3282–3284 (2010).
14. D. L. Marks, C. Vinegoni, J. S. Bredfeldt, and S. A. Boppart, "Interferometric differentiation between resonant coherent anti-Stokes Raman scattering and nonresonant four-wave-mixing processes," Appl. Phys. Lett. **85**(23), 5787–5789 (2004).
15. F. Ganikhanov, C. L. Evans, B. G. Saar, and X. S. Xie, "High-sensitivity vibrational imaging with frequency modulation coherent anti-Stokes Raman scattering (FM CARS) microscopy," Opt. Lett. **31**(12), 1872–1874 (2006).
16. B. G. Saar, G. R. Holtom, C. W. Freudiger, C. Ackermann, W. Hill, and X. S. Xie, "Intracavity wavelength modulation of an optical parametric oscillator for coherent Raman microscopy," Opt. Express **17**(15), 12532–12539 (2009).
17. B. C. Chen, J. Sung, and S. H. Lim, "Chemical imaging with frequency modulation coherent anti-Stokes Raman scattering microscopy at the vibrational fingerprint region," J. Phys. Chem. B **114**(50), 16871–16880 (2010).
18. K. Chen, T. Wu, H. Wei, and Y. Li, "Dual-soliton Stokes-based background-free coherent anti-Stokes Raman scattering spectroscopy and microscopy," Opt. Lett. **41**(11), 2628–2631 (2016).
19. F. Ganikhanov, S. Carrasco, X. Sunney Xie, M. Katz, W. Seitz, and D. Kopf, "Broadly tunable dual-wavelength light source for coherent anti-Stokes Raman scattering microscopy," Opt. Lett. **31**(9), 1292–1294 (2006).
20. O. Burkacky, A. Zumbusch, C. Brackmann, and A. Enejder, "Dual-pump coherent anti-Stokes-Raman scattering microscopy," Opt. Lett. **31**(24), 3656–3658 (2006).
21. K. J. Blow, N. J. Doran, and D. Wood, "Polarization instabilities for solitons in birefringent fibers," Opt. Lett. **12**(3), 202–204 (1987).
22. E. R. Andresen, P. Berto, and H. Rigneault, "Stimulated Raman scattering microscopy by spectral focusing and fiber-generated soliton as Stokes pulse," Opt. Lett. **36**(13), 2387–2389 (2011).
23. A. F. Pegoraro, A. Ridsdale, D. J. Moffatt, Y. Jia, J. P. Pezacki, and A. Stolow, "Optimally chirped multimodal CARS microscopy based on a single Ti:sapphire oscillator," Opt. Express **17**(4), 2984–2996 (2009).
24. I. Rocha-Mendoza, W. Langbein, P. Watson, and P. Borri, "Differential coherent anti-Stokes Raman scattering microscopy with linearly chirped femtosecond laser pulses," Opt. Lett. **34**(15), 2258–2260 (2009).
25. L. Brückner, T. Buckup, and M. Motzkus, "Enhancement of coherent anti-Stokes Raman signal via tailored probing in spectral focusing," Opt. Lett. **40**(22), 5204–5207 (2015).
26. L. Brückner, T. Buckup, and M. Motzkus, "Exploring the potential of tailored spectral focusing," J. Opt. Soc. Am. B **33**(7), 1482–1491 (2016).
27. W. Min, C. W. Freudiger, S. Lu, and X. S. Xie, "Coherent nonlinear optical imaging: beyond fluorescence microscopy," Annu. Rev. Phys. Chem. **62**(1), 507–530 (2011).
28. H. A. Rinia, K. N. Burger, M. Bonn, and M. Müller, "Quantitative label-free imaging of lipid composition and packing of individual cellular lipid droplets using multiplex CARS microscopy," Biophys. J. **95**(10), 4908–4914 (2008).

1. Introduction

Raman microscopy has been extremely successful in visualizing the chemical changes and distribution of species within soft and complex materials, including polymeric and biological samples, as a powerful label-free technique [1,2]. It especially provides a high level of sensitivity and specificity to identify disease related chemical changes [3]. The conventional spontaneous Raman imaging methods bear two major weaknesses, including weak signal intensity and an often strong fluorescence background in the same spectral range. The discrimination of subtly different states of cells and tissues relying on multiple Raman peaks within the weakly scattering fingerprint region (<1,800 cm^{-1}) generally requires long integration time in the order of seconds per spectrum [4], seriously limiting the use of Raman spectroscopy in high-speed imaging. To bolster the inherently weak Raman scattering process, coherent Raman techniques have been developed, which coherently populate

Biomedical Optics EXPRESS

selected vibrational states of molecules through their nonlinear response to multiple pulsed laser fields. Successful techniques for microscopy include coherent anti-Stoke Raman scattering (CARS) microscopy [5] and stimulated Raman scattering (SRS) microscopy [6]. In both cases, video-rate imaging of single Raman bands can be achieved with narrow spectral bandwidth [7,8], but suffers from limitations in breadth and speed of laser tuning rates. With respect to the multiplex or broadband CARS or SRS spectroscopy and imaging, there is considerably more information contained throughout an entire spectrum than at just a single frequency within that spectrum [9,10]. This advantage is more useful for qualitative discrimination of many overlapping peaks, in general, and more amenable to quantitative analysis of variations in the spatial distribution of different molecules in the sample.

In order to further reconcile the bandwidth and resolution conflict of broadband lasers in the broadband (multiplex) CARS, Raman spectrum can be acquired by scanning the time delay between the two pulses when they are appropriately chirped. This is known as the spectral focusing approach [11], which concentrates most of the optical power into a single Raman vibrational mode, thereby providing a flexible way to optimize the spectral resolution and signal-to-noise ratio. However, a well-known background from nonresonant (NR) CARS contributions severely limits the sensitivity and specificity of multiplex CARS, which does not carry chemically specific information. The NR background can further distort the resonant signal of interest, which has limited the extent to which CARS microscopy has been used as a fully quantitative imaging technique. It especially renders quantitative CARS hyperspectral imaging on target samples exceedingly difficult in the fingerprint spectral region where molecules present their unique vibrational signature with lower cross section than the frequently used C–H stretch [9]. Some approaches have been devised to minimize the NR background contribution to the measured multiplex CARS spectrum [12–17]. Frequency modulation (FM) CARS, has proven to be an effective way to eliminate the nonresonant background, relying on the different spectral shapes of the resonant CARS and NR signals [15–17]. If one can perform a differential measurement with slightly shifted excitation frequencies, the nonresonant background can be eliminated in the FM-CARS scheme. In the previously demonstrated narrow FM-CARS microscopy methods, one needs either two different pump lasers that are switched by a Pockels cell [15] or a sophisticated optical parametric oscillator (OPO) that can modulate the frequency of the output pulses [16]. With respect to the broadband CARS, Chen et al. firstly proposed a new FM-CARS version by combination of fast frequency modulation of time-delay between pump and Stokes pulses and lock-in signal detection for quantitative analysis of unsaturation composition in mixtures of fatty acids [17]. Hence, sophisticated laser systems or pulse-scan system were required to perform the necessary fast frequency modulation in beam-scanning microscopy for the above-mentioned methods, yielding a complex and costly setup. The challenge is then to find a way of suppressing the NR signals of multiplex CARS, while beating the inaccessibility and complexity of conventional modulation system. Very recently, we established a new all-fiber-generated dual-soliton Stokes based scheme for background-free CARS under the spectral focusing mechanism [18], without any additional modulation. This scheme, termed as DS-CARS, takes full advantage of the all-fiber-based source technology which could be used in less favorable environments while being compact and inexpensive.

In this article, we establish a dual-soliton Stokes based multiplex and background-free CARS method capable of quantifying the spatial information of densities and chemical composition within inhomogeneous samples. We show that our method not only removes the NR background but also generates Raman-like CARS signals at multiple characteristic vibrational frequencies in the fingerprint region. We demonstrate that the degree of unsaturation of mixture lipid droplets can be determined with a well-defined correlation between the vibration ratio of C = C/CH_2 and the chemical concentrations. We further demonstrated that, the spatially inhomogeneous distribution of lipid droplets can be quantitatively visualized using the degree of acyl chain unsaturation for contrast in the

Biomedical Optics EXPRESS

hyperspectral CARS images. We believe that the powerful combination compact excitation source and background-free capability can greatly simplify multiplex CARS spectroscopy measurements and extend the practicality of quantitative CARS microscopy for studying material and biological systems.

2. Materials and methods

2.1 Dual-soliton pulse generation

The current gold-standard laser system for CARS microscopy is synchronized picosecond (ps) mode-locked solid-state oscillators [19], or synchronously pumped ps OPOs [20]. Free space lasers generally require a stable environment or active feedback, whereas an all-fiber source could be used in less favorable environments while being more compact and inexpensive. Here we show, by exploring the potential of high birefringence of polarization-maintaining photonic crystal fiber (PM-PCF), that a new version of fiber-generated Stokes pulse can be harnessed for background-free CARS spectroscopy and microscopy [18]. This birefringence has the potential to simultaneously generate two continua (two soliton pulses) with orthogonal polarizations, allowing for an extra degree of freedom in tuning the properties of the supercontinuum.

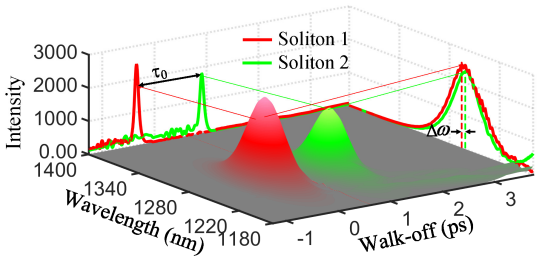

Fig. 1. Simulation of dual-soliton output of the PM-PCF when the angle between the input polarization and the fast axis is 42°. Frequency separation between soliton 1 and 2 is about $\triangle\omega$ = 1.5nm; Temporal walk-off is about τ_0 = 1.3ps.

Governed by the coupled vector nonlinear Schrödinger equations [21], numerically simulated results in Fig. 1 qualitatively display the generated spectra and soliton pulse profiles. When the input polarization isn't parallel to the fast or slow axes, contour plots of the spectra provides an unambiguous proof that the generated spectrum is a linear combination of two continua generated separately along the two principal axes. Indeed, spectral components along one axis are not coupled to those in the other axis. This is attributable to the different dispersion characteristics of the two eigenpolarizations, thus leading to the temporal walk-off of this dual-soliton τ_0. It is worth noting that both frequency separation and temporal interval between dual-soliton pulses can be easily adjusted by rotating the input polarization. Soliton 2 shifts just about 1.5nm (~10 cm^{-1}) relative to soliton 1, towards to shorter wavelength, and the temporal interval is about 1.3ps. Due to the balance between anomalous dispersion and the Kerr nonlinearity [22], both soliton 1 and 2 are nearly transform-limited.

2.2 Spectral focusing CARS

In the CARS process, molecules are excited by two input light fields, a pump pulse and a Stokes pulse, whose frequency difference is chosen to match the frequency of Raman active transitions. If transform limited femtosecond pulses are used, the signal size increases at the expense of reduced spectral resolution. A straightforward way, known as spectral focusing method is to equally apply a linear temporal chirp on both pump and Stokes pulses to resolve the conflict. For linearly chirped pulses under the stationary phase approximation, the pump and Stokes electric field can be described by:

Biomedical Optics EXPRESS

$$E_P(t) = E_{P0}(t)e^{-i\omega_{P0}t - i\alpha t^2} + C.C. \tag{1}$$

$$E_S(t-\Delta t) = E_{S0}(t-\Delta t)e^{-i\omega_{S0}(t-\Delta t) - i\alpha(t-\Delta t)^2} + C.C. \tag{2}$$

where E_P and E_S are the complex field envelopes and E_{P0} and E_{S0} represent the absolute field amplitude. ω_{P0} and ω_{S0} are the center frequency of pump and Stokes pulses and Δt is the delay between them. α is the common chirp parameter. The frequency components of the two beams are thereby stretched in time, thus leading to the instantaneous frequencies: $\omega_P(t) = \omega_{P0} + 2\alpha t$ and $\omega_S(t) = \omega_{S0} + 2\alpha(t\text{-}\Delta t)$, respectively. Let us consider the nonlinear vibrational excitation field, $A(t)$, by chirped pump and Stokes pulses [11, 17, 23]:

$$\begin{aligned} A(t) &= E_P(t)E_S^*(t-\Delta t) \\ &= E_{P0}(t)E_{S0}^*(t-\Delta t)e^{-i(\omega_{P0}-\omega_{S0}+2\alpha\Delta t)t} \times e^{-i(\omega_{S0}-\alpha\Delta t)\Delta t}. \end{aligned} \tag{3}$$

Obviously, equal linear chirp on both pump and Stokes pulses creates a constant, narrowed, instantaneous frequency difference (IFD) as $\Omega_{\text{IFD}} = \omega_{p0}\text{-}\omega_{s0} + 2\alpha\Delta t$, which drives a single Raman coherence [23–26]. It also offers a route at tuning the IFD within the spectral width of the chirped pulses by simply adjusting their relative time delay, allowing to perform broadband CARS spectroscopy without tuning the laser sources. Most importantly, one can achieve the best compromise between spectral resolution and signal strength for CARS microscopy when the time durations of the pump and Stokes pulses are similar to the vibrational dephasing time of molecules (a few picoseconds) [23].

2.3 Dual-soliton CARS

The temporal walk-off dual-soliton pulses can be intrinsically applied to the spectral focusing scheme, which performs CARS spectroscopy by sequentially sweeping the interpulse delay between pump and Stokes pulses. In the spectral focusing mechanism, a single Raman level can be excited by multiple pairs of pump and Stokes frequency components, accompanying with NR nonspecific four-wave-mixing signal at the same frequency as schematically illustrated in Fig. 2(a) and 2(b). The total CARS response can be described as the sum of resonant third-order nonlinear polarization $P_{\text{R}}^{(3)}$ and the NR one $P_{\text{NR}}^{(3)}$. The detected CARS signal $I_{CARS}(\omega_{as})$ at anti-Stokes frequency (ω_{as}) is therefore proportional to [9]:

$$\begin{aligned} I_{CARS}(\omega_{as}) &\propto \left|P^{(3)}(\omega_{as})\right|^2 = \left|P_{NR}^{(3)} + P_R^{(3)}(\omega_{as})\right|^2 \\ &\propto \left|P_{NR}^{(3)}\right|^2 + \left|P_R^{(3)}(\omega_{as})\right|^2 + 2P_{NR}^{(3)}\text{Re}\left[P_R^{(3)}(\omega_{as})\right]. \end{aligned} \tag{4}$$

$P_{NR}^{(3)}$ is real, chemically-nonspecific typically assumed to be slowly varying in frequency (although not necessarily constant). As described by the last term of Eq. (4), the non-resonant background electric field distorts the CARS spectrum due to its constructive and destructive interference with the resonant vibrational contribution, $\text{Re}\{P_R^{(3)}(\omega_{as})\}$, on the red and blue sides of the Raman peak, respectively [26]. The resonant nonlinear polarization $P_{\text{R}}^{(3)}(\omega_{as})$ can be further written in a more tractable form [9]:

$$P_R^{(3)}(\omega_{as}) \propto \{\chi_{\text{R}}^{(3)}[E_s(\omega_{as}) \star E_p(\omega_{as})] \otimes E_{pr}(\omega_{as}). \tag{5}$$

$$\chi_{\text{R}}^{(3)} = \chi_R^{(3)}(\omega_{as};\omega_p,-\omega_s,\omega_{pr}) = \sum_j \frac{NA_j}{\Omega_j - (\omega_p - \omega_s) - i\Gamma_j}. \tag{6}$$

Biomedical Optics EXPRESS

where $\star$ and $\otimes$ are the cross-correlation and convolution operations, respectively; $E_p(\omega_{as})$, $E_s(\omega_{as})$ and $E_{pr}(\omega_{as})$ are the pump, Stokes and probe electric field, respectively; $\chi_R^{(3)}$ is the nonlinear susceptibility for the resonant components. ω_p, ω_s and ω_{pr} are the pump, Stokes and probe frequencies, respectively;A_j, Ω_j, and Γ_j are the amplitude, frequency, and line width of the j^{th} vibrational mode and N is the number of scatterers per unit volume.

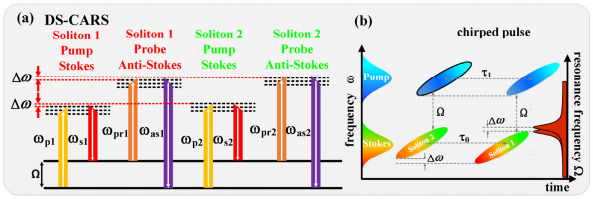

Fig. 2. (a) Energy-level scheme of the DS-CARS process under spectral focusing mechanism. (b) Principle of the spectral focusing and DS-CARS in the time-frequency plane. Note that there is only one pump that is scanned in time from soliton 1 all the way to soliton 2. τ_0 is the temporal walk-off of the dual-soliton pulses; τ_1 is the delay interval.

In the Dual-soliton CARS scheme, the Raman level Ω can be excited twice while scanning the interpulse delay between the pump and the Stokes beam shown in Fig. 2(a). So, we can acquire CARS signals at different time-delay: $I_{CARS1}(\omega_{as}, \omega_{as1})$ and $I_{CARS2}(\omega_{as}, \omega_{as2})$. By combining the time and frequency picture in Fig. 2(b), the effect of the frequency separation between the two soliton pulses on the vibrational coherence and especially on the signal generation can be promptly understood. As revealed by Fig. 2(b), the delay interval τ_1 is not equal to the temporal interval of two TL soliton pulses τ_0, since soliton 2 shifts to higher frequency by a slight amount of $\Delta\omega$. Then the excellent linear correlation between the time delay and frequency components of the chirped pump (or probe) pulse ensures the same amount of shift between ω_{pr1} and ω_{pr2}, further leading to the frequency difference of the two anti-Stokes signals ω_{as2}-ω_{as1} = $\Delta\omega$ as illustrated in Fig. 2(a). This frequency modulation with two excitation wavelengths shifted by an amount comparable to the bandwidth of the measured Raman bands has been demonstrated as an effective way to eliminate the large backgrounds [17,24]. Dual-soliton CARS scheme is therefore naturally endowed with this capability to suppress the NR signals. In the scenario of weak or dilute analytes, $\left|P_R^{(3)}(\omega_{as})\right|^2 << \left|P_{NR}^{(3)}\right|^2$, and Eq. (4) simplifies to $I_{CARS}(\omega_{as}) \propto \left|P_{NR}^{(3)}\right|^2 + 2P_{NR}^{(3)}\,\mathrm{Re}\left[P_R^{(3)}(\omega_{as})\right]$.We can then exhibit a difference CARS spectrum between $I_{CARS1}(\omega_{as}, \omega_{as1})$ and $I_{CARS2}(\omega_{as}, \omega_{as2})$.

$$\Delta I_{CARS}(\omega_{as}) \propto 2P_{NR}^{(3)}\left\{\mathrm{Re}\left[P_R^{(3)}(\omega_{as},\omega_{as1})\right]-\mathrm{Re}\left[P_R^{(3)}(\omega_{as},\omega_{as2})\right]\right\} \propto N. \qquad (7)$$

The DS-CARS response is then linear in concentration amplified by the NR background without any offset from the strong NR contribution. We will further elaborate this linear correlation with simulations in Fig. 3. Two simulated CARS signals generated by soliton 1 and 2 with an appropriate frequency separation are both distorted by the nonresonant background in Fig. 3(a). However, the output lineshape of the difference spectrum between the two distorted CARS signals looks close to that of spontaneous Raman scattering. More importantly, the DS-CARS become linearly proportional to sample concentration. This linear dependence can be clearly demonstrated in the case of different Raman peak width (5, 15 and 10 cm^{-1}) and frequency separations (4, 8, 10, 12 and 16 cm^{-1}) in (b) and (c), respectively. This is due to the fact that our DS-CARS measures the cross term $2P_{NR}^{(3)}\,\mathrm{Re}\left[P_R^{(3)}(\omega_{as})\right]$ in Eq. (7). It should be noted that, when the resonant signal is comparable with or larger than the nonresonant one which beyond the heterodyne ($\left|P_R^{(3)}(\omega_{as})\right|^2 << \left|P_{NR}^{(3)}\right|^2$) limit in Fig. 3(d), this

Biomedical Optics EXPRESS

linear relationship still holds ($\left|P_R^{(3)}(\omega_{as})\right| = 1.6\left|P_{NR}^{(3)}\right|$, $R^2 = 1$). Our simulation even reveals that one can find a reliable linear estimation of the concentration of dilute analytes ($R^2 = 0.975$) in the case of $\left|P_R^{(3)}(\omega_{as})\right| = 10\left|P_{NR}^{(3)}\right|$, which allows a broader application of quantitative DS-CARS spectroscopy and microscopy. Besides, a smaller frequency separation between soliton 1 and 2 generally leads to the increase of the spectral resolution of the DS-CARS, yet the decrease of the intensity as shown in Fig. 3(c). In order to maximize the spectral resolution of DS-CARS signals with minimum loss of its peak intensity, the frequency separation between the two Stokes pulses should be matched with the Raman mode to be probed.

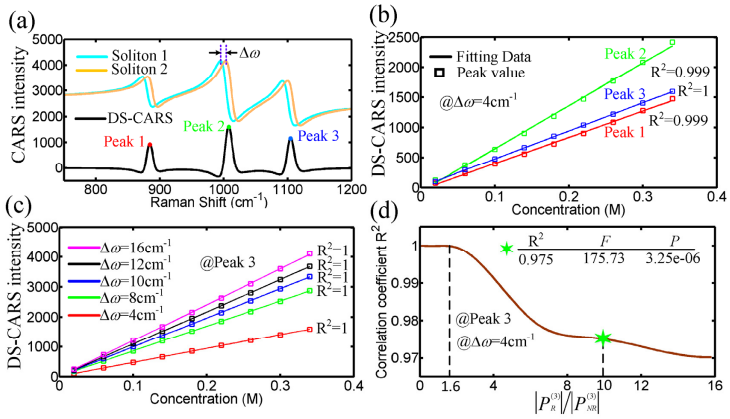

Fig. 3. (a) DS-CARS spectrum (black) with three peaks is obtained from the difference of the two simulated CARS signals by soliton 1 and 2. (b) and (c) Simulated effect of peak location of DS-CARS (b) and spectral separation of the dual-soliton (c) on the linear correlation between Peak intensity and concentration of dilute analytes. (d) The correlation coefficient R^2 against the ratio of resonant and nonresonant contribution. The marker (green hex star) represents a nonresonant contribution about 100 times weaker than the resonant contribution. *F* = the F-test value, *P* = statistical significance.

2.4 Experimental setup

The implementation of DS-CARS proceeds as presented in Fig. 4(a) [18]. A home-built Yb-doped fiber laser with an output of 2W average power at 100 MHz repetition rate was used as the primary source. This laser output was split into the pump and the Stokes paths. For efficient Stokes generation, about 650mW is coupled into a 192 cm highly nonlinear PM-PCF (coupling efficiency~30%).The continuum redshifts to about 1280nm so as to cover most of the fingerprint region from 1150 to 1800 cm^{-1}, by adjusting the input power to the PCF using a half wave-plate and polarizing beam splitter combination. By rotating the input polarization, the generated spectrum at the fiber output actually consists of a superposition of the spectra generated independently by the two eigenpolarization modes, which is termed as Soliton 1 (red line) and Soliton 2 (green line) in Fig. 4(b). These results are in good agreement with the simulated contour plots in Fig. 1. The temporal walk-off (τ_0) and the frequency separation ($\triangle\omega$) between two soliton pulses are 1.4ps and $10cm^{-1}$, respectively. SF57 glass rods with different length are added to ensure that the same amount of linear positive chirp are applied to both pump and Stokes beam. After traveling through these high-index glass rod, the pulse durations of pump and Stokes pulses are measured to be 2.2ps and 1.4ps, respectively with an autocorrelator (APE-Berlin). It is worth noting that both the frequency separation ($\triangle\omega$) and the degree of linear chirp are chosen considering the Raman line width of the mode to be probed. A motorized delay line is inserted into the pump beam to scan the delay between the two pulse trains. These two beams are overlapped in space by a dichroic mirror and sent into a custom-made scanning microscope with a near-infrared optimized excitation objective lens

Biomedical Optics EXPRESS

(NA = 0.65, LCPLN50XIR, Olympus) and the collection objective is the same as the excitation one. The signal at anti-Stokes frequency is detected in the forward direction by means of an imaging spectrograph (IsoPlane160, Princeton Instruments) attached with a back-illuminated, deep depletion CCD (PIXIS1024BR, Princeton Instruments). For imaging, the sample is raster scanned. Most of CARS measurements in this work are performed with the pump and Stokes powers of 40.0mW and 12.0mW ($I_{\text{soliton 1}}$ = 6.5mW, $I_{\text{soliton 2}}$ = 5.5mW), respectively. Prominent spontaneous Raman peaks of ethanol are used to calibrate the linear coefficient between the optical delay and Raman wavenumber. Linear fitting of these Raman peaks to corresponding optical delays in DS-CARS measurements results in a calibration curve which can be used to determine Raman shift at any interpulse delay (Fig. 4(c)).

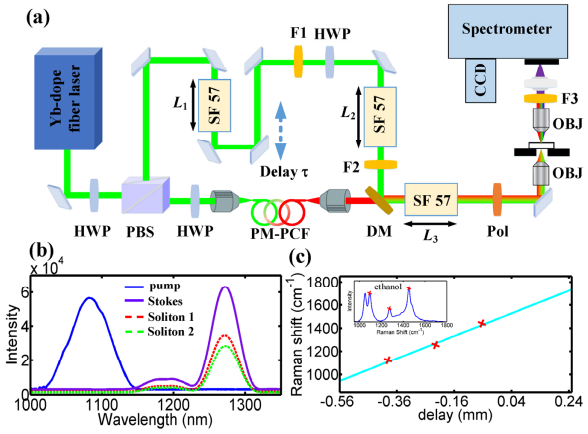

Fig. 4. (a) Sketch of the experimental setup: HWP, half wave-plate; PBS, polarizing beam splitter; PCF, photonic crystal fiber; F1, F2, long-pass filter; F3, short-pass filter; Pol, polarizer ; SF57, SF-57 glass rod; DM, dichroic mirror; OBJ, objective lenses; L_1 = 30mm, L_2 = 108mm, L_3 = 200mm. (b) The output spectra of Stokes and pump; Stokes profile is a linear combination of soliton 1 and 2. (c) Calibration of Raman shift with respect to pump-Stokes pulse delay using a set of Raman peaks of ethanol; insets showing the spontaneous Raman spectra of ethanol with three peaks to be used in the calibration.

2.5 Sample preparation

For multiplex DS-CARS acquisition, a kind of polymer film, polyethylene glycol terephthalate (PET) with the thickness of 200μm was directly used. The fatty acids used in this work are fish oil (Nature's Bounty, USA), olive oil (Betis, Spainsh) and oleic acid (Sigma-Aldrich) and used without further purification. For quantitative identification of lipid unsaturation, different proportions of fish oil were directly incorporated into olive oil. For quantitative DS-CARS imaging, oil droplets are prepared in the following way [17]: 0.1 g of each oil is mixed with 0.1 g of Triton X-100 (Sigma-Aldrich) and stirred for 10 min, and 10 mL of water is added to the mixture, which is stirred further for 2 h. Separately prepared olive and fish oil droplets are mixed afterward. For all the liquid samples, a drop of solution was pipetted inside a 120μm thick imaging spacer (GraceTMBio-Lab SecureSealTM) glued on a glass slide (1 mm thick) in order to create a chamber, which was sealed by a second coverslip (0.13mm thick) on top.

3. Results and discussion

3.1 Multiplex DS-CARS spectra of polymer film

We first address the background-free multiplex CARS spectra in the dual-soliton scheme. Figure 5(a) shows the measured CARS spectrograms of PET film with the thickness of 200μm. We are bringing clear evidences that the two soliton Stokes pulses together with one pump pulse can excite a Raman level subsequently while scanning the interpulse delay

Biomedical Optics EXPRESS

between the pump and the Stokes beam, also as illustrated in Fig. 2(a) The true CARS spectra are extracted from the three-dimensional spectrograms as the amplitude along the time-delay by integrating the total power of each anti-Stokes spectrum from the spectrometer. As shown in Fig. 5(b), CARS signals produced from both soliton 1 and 2 present distorted and typically dissipative spectral lineshape, which is ascribed to the strong NR backgrounds and well-understood in the CARS community. In the DS-CARS scheme the pump pulse scans the two Stokes soliton pulses at different delay-time and the delay interval is about τ_1 in (b). It is worth noting that τ_1 is not equal to the temporal interval of two soliton pulses τ_0, because the frequency separation of soliton 1 and 2 translates to difference of excited Raman frequency. After shifting the CARS spectra of soliton 2 in the time domain by the amount of τ_0, the underlying broad NR background can be subtracted from the difference between these two CARS signals, and its output is almost background–free and more resolvable (Fig. 5(c)). DS-CARS spectra of PET is almost identical to its spontaneous counterparts except for relative intensity differences at low and high wavenumbers due to decreased pulse overlap [10]. This intensity variation is always constant and can be removed by calibration against the known spontaneous Raman signals if needed. Figure 5(d) shows the intensity calibrated DS-CARS spectra, in which the spectral positions and FWHMs of different Raman resonance match very well with the spontaneous spectrum, allowing quantitative analysis in CARS spectroscopy and microscopy.

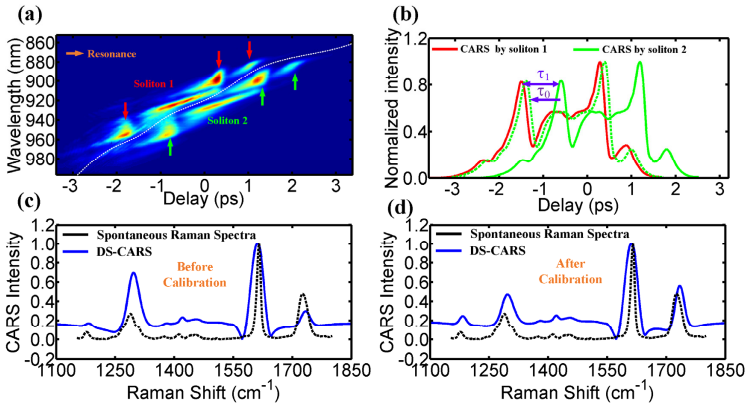

Fig. 5. (a) Measured CARS spectrograms of PET as a function of pulse delay and the signal wavelength. (b) CARS spectra generated from soliton 1 and soliton 2 and shift I_{CARS2} towards I_{CARS1} by the amount of τ_0. (c) Difference CARS signals between I_{CARS2} and I_{CARS1} (DS-CARS) and the spontaneous Raman spectra of PET. (d) Intensity calibrated DS-CARS and the spontaneous Raman spectra of PET. τ_0 is the temporal walk-off of the dual-soliton pulses; τ_1 is the delay interval.

3.2 Quantitative chemical identification of fatty acids

Understanding the diverse biological functions of lipid droplets and their role in the development of metabolic diseases requires the number of double C = C bonds within lipid acyl chains, i.e., the degree of unsaturation. Clearly, quantitative spatial and temporal information on the degree of lipid unsaturation would greatly contribute to our understanding of metabolic diseases and the influence of nutritional factors [28]. Oleic acid is a monounsaturated omega-9 fatty acid with 18-carbon chain and one C = C double bond (18:1). According to the manufacture label of the olive oil used in this experiment, it contains 14, 7, and 79% of saturated, polyunsaturated, and monounsaturated fatty acid, respectively. The major component in olive oil is oleic acid. For the fish oil, 30% of its content is a mixture of eicosapentanoic acid (20:5), docosahexanoic acid (22:6) and other polyunsaturated fatty acids according to the manufacture's label. Figure 6 shows the DS-CARS and spontaneous Raman spectra of fish oil, olive oil and oleic acid. The originally measured CARS spectra by soliton1

Biomedical Optics EXPRESS

and 2 are severely distorted by the nonresonant background in Fig. 6(a), while DS-CARS produces Raman-like CARS signals in (b). Since these spectra contain rich information from multiple characteristic vibration peaks such as olefinic C = C and methylene CH_2 deformations, background-free DS-CARS is more likely to identify molecular structures by quantitative spectral analysis. Besides, difference based DS-CARS is even more resolved than the spontaneous Raman spectra in the crowded Raman region at 1260 and 1300 cm^{-1}. The spectral resolution of DS-CARS can be estimated at 15 cm^{-1} from the two Raman peaks.

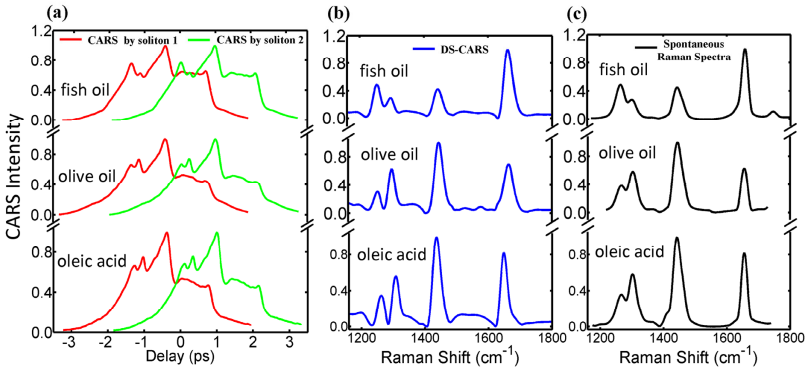

Fig. 6. (a) The originally measured CARS spectra of fish oil, olive oil and oleic acid by soliton1 and 2 with strong nonresonant background. (b) and (c) DS-CARS and spontaneous Raman spectra of the same fatty acids. Each trace is vertically displaced for clarity.

In Fig. 6(b), the 1260 and 1300 cm^{-1} peaks are assigned to in-plane olefinic hydrogen bending (1260 cm^{-1}) and methylene twisting deformation (1300 cm^{-1}) [17].The former increase with the numbers of C = C double bonds; the latter increase with the number of C-C single bonds. The resonances at 1650 and 1450 cm^{-1} originated from the ν(C = C) stretching and $\delta(CH_2)$ deformation vibrations, respectively. The signal at 1650 cm^{-1} was directly proportional to the concentration of C = C bonds, and the1450 cm^{-1} resonance can be used as a measure of total fatty-acid concentration [26]. Obviously, the peak ratios of 1260 and 1300 cm^{-1} (I_{1260}/I_{1300}) and 1450 and 1650 cm^{-1} ((I_{1450}/I_{1650})) provide a quantitative measure for the degree of lipid-chain unsaturation: C = C/CH_2 and CH_2/C = C, respectively. Low unsaturation level of olive oil shows $I_{1260}/I_{1300}<1$ and $I_{1450}/I_{1650}>1$. On the other hand, high unsaturation level of fish oil exhibits $I_{1260}/I_{1300}>1$ and $I_{1450}/I_{1650}<1$ as shown in Fig. 7(a).

In order to verify the linear dependence on the sample concentration experimentally, as we demonstrated in Fig. 4, we further test the variation of peak ratios (I_{1260}/I_{1300} and I_{1450}/I_{1650}) with the fish fraction in the fish/olive mixture oil droplets. On the basis of the theoretical analysis in Eq. (7), we can express the peak ratio in the mixture oil as

$$f_{I_{1260}/I_{1300}}(m)=\frac{mI_{1260}^{fish}+(1-m)I_{1260}^{olive}}{mI_{1300}^{fish}+(1-m)I_{1300}^{olive}}. \tag{8}$$

$$f_{I_{1450}/I_{1650}}(m)=\frac{mI_{1450}^{fish}+(1-m)I_{1450}^{olive}}{mI_{1650}^{fish}+(1-m)I_{1650}^{olive}}. \tag{9}$$

where m is the fish fraction in the fish/olive mixture oil droplets (sample concentration). $f_{I_{1260}/I_{1300}}$ and $f_{I_{1450}/I_{1650}}$ represent the peak ratio of I_{1260}/I_{1300} and I_{1450}/I_{1650}, respectively, in the oil mixture. I_x^{fish} and I_x^{olive} represent the peak-intensity value at Raman resonance x (x = 1260, 1300, 1450 and 1650) of pure fish and olive oil, respectively, which are key parameters of the two equations. Specifically, these parameters are obtained by nonlinearly fitting experiment

Biomedical Optics EXPRESS

data as: $I_{1260}^{fish}=1.72$, $I_{1300}^{fish}=1.05$, $I_{1450}^{fish}=2.79$, $I_{1650}^{fish}=6.76$ and $I_{1260}^{olive}=1.01$, $I_{1300}^{olive}=2.11$, $I_{1450}^{olive}=7.39$, $I_{1650}^{olive}=5.21$ using the theoretical Eqs. (10) and (11). It is apparent from Fig. 7(b) that a good correlation of two peak ratios (I_{1260}/I_{1300} and I_{1450}/I_{1650}) and the fish fraction in fish/olive mixture can be established. More importantly, when the two experimental data are compared with theoretical fitting curves of Eq. (8) and (9), it is noticeable the proximity between experimental results and theoretical plot. Indeed, the calculated average relative error between the theoretical and experimental results are 0.007% and 0.016% and the maximum difference are of 3.3% and 2.9% in the entire range of concentration variation for I_{1260}/I_{1300} and I_{1450}/I_{1650}, respectively. These features provide rich chemical information about acyl chains of fatty acids and lipids to determine the unsaturation level. They serve as quantitative means of chemical selectivity in oil droplet imaging in the next sections.

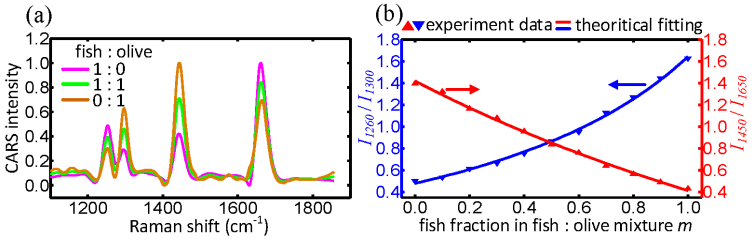

Fig. 7. Illustration of quantitative nature of multiplex DS-CARS. (a) DS-CARS spectra of fish/olive mixtures in the fingerprint region. The fish/olive molar ratio is indicated. (b) Comparison between experiment value of I_{1260}/I_{1300} and I_{1450}/I_{1650} in the mixture oil (red and blue triangle) and theoretical fitting curve (red and blue solid line) as a function of fish fraction in fish/olive mixture.

Background-free multiplex CARS imaging can be used to quantitatively map the spatial variations in the level of lipid unsaturation and acyl-chain order of different oil droplets. Figure 8(a) and 8(b) show the DS-CARS images of a mixture of olive and fish oil droplets at 1260 and 1300 cm^{-1}, respectively. The main difference between their chemical structures is the degree of unsaturation in their acyl chains. Olive oil consists of oleic acid (18:1) primarily (79%), while fish oil contains a large amount (30%) of polyunsaturated fatty acids such as EPA (20:5) and DHA (22:6). Note that both oils possess vibrational peaks at 1260 and 1300 cm^{-1}. Because of the high unsaturation level, one can see larger signals from fish oil droplets than the olive ones at 1260 cm^{-1} at droplet A in Fig. 8(a). On the other hand, the olive oil droplet B is a little brighter than the fish ones in Fig. 8(b). However, brightness contrast in microscopy may lead to false chemical identification. For example, the droplet marked with arrows in Fig. 8(a) is a fish oil droplet positioned vertically off from the laser focus. Its apparent signal strength at 1260 cm^{-1} is similar to that of the olive oil droplet. The olive oil droplet marked with arrows in Fig. 8(b) also suffers from this problem. So, spatial and temporal information of lipid droplets can be easily obfuscated by the qualitative visual inspection. Background-free multiplex CARS has the potential to be used to quantify the degree of lipid-chain unsaturation and then the two oil droplets in microscopy, using the peak ratio (I_{1260}/I_{1300}). We compare the CARS images at 1260 cm^{-1} (Fig. 8(a)) and 1300 cm^{-1} (Fig. 8(b)) and take the ratio image as shown in Fig. 8(c). It can quantitatively and clearly distinguish these two different oil droplets. We find that the intensity ratios of 1260 and 1300 cm^{-1} peaks (I_{1260}/I_{1300}) are ~1.6 and ~0.48 for fish and olive oils, respectively.

Biomedical Optics EXPRESS

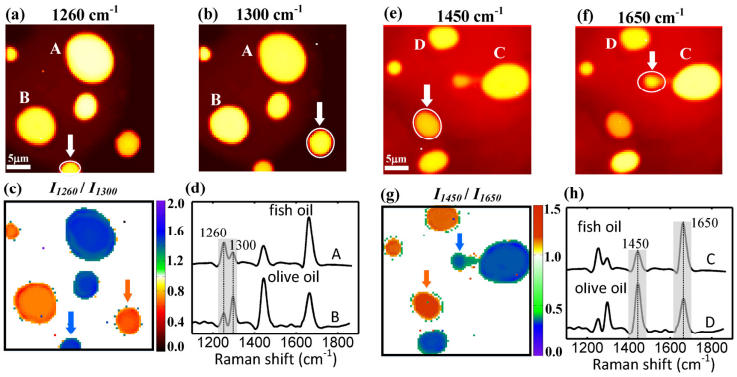

Fig. 8. DS-CARS images at (a) 1260 cm^{-1}, (b) 1300 cm^{-1}, (e) 1450 cm^{-1} and (f) 1650 cm^{-1} of a mixture of fish and olive oil droplets. Image 50 × 50 pixels, pixel time 50 ms. The droplets marked with arrows are difficult to identify in (a), (b), (e) and (f). (c) and (g) Intensity ratio image of 1260 cm^{-1} over 1300 cm^{-1} (I_{1260}/I_{1300}) and 1450 cm^{-1} over 1650 cm^{-1} (I_{1450}/I_{1650}). Fish and olive oil droplets appear blue and reddish yellow, respectively. (d) and (h) DS-CARS spectra of the oil droplets marked as A, B, C and D in parts (a), (b), (e) and (f), respectively. All the traces in (d) and (h) are vertically displaced for clarity.

We have also taken the CARS images of the same samples in different field of view at 1450 and 1650 cm^{-1} in Fig. 8(e) and 8(f) and performed the ratio image (I_{1450}/I_{1650}) in Fig. 8(g). As mentioned above, the resonances at 1650 cm^{-1} comes from the C = C double bond stretching and the I_{1450}/I_{1650} serves as another indicator of lipid unsaturation level over broader sample ranges. Fish oil droplets exhibit I_{1450}/I_{1650} ~0.42 and olive ones exhibit I_{1450}/I_{1650} ~1.44. Therefore, one can also clearly identify each droplet by the peak intensity ratio like I_{1260}/I_{1300}, avoiding false interpretation of local chemical components. It is worth noting that the spot by the blue arrow, which is actually a fish droplets shows green color with low signal strength in (g), because it has small size and is positioned slightly off from the laser focus. The validity of the background-free multiplex CARS microscopy can be seen from the quantitative images of both Fig. 8(c) and 8(g) and the results are in good agreement with the previously reported work [17,28].

We can also implement microspectroscopy while taking CARS images. Figure 8(d) and 8(h) show DS-CARS spectra taken at the droplets A, B and C, D. We position the laser focus at the point of interest and scan the time delay to obtain these spectra. Thus, we are able to not only acquire chemical images at several important frequencies in real-time but also perform microspectroscopy at a few positions of interest. Combination of multiple frequency imaging and microspectroscopy will be a powerful tool in the study of complex samples such as cells and tissues, offering more chemical sensitivity and selectivity.

4. Conclusion

The combination of the high specificity of background-free CARS with rich information from multiple characteristic vibration peak in multiplex CARS spectra allows for excellent capability in quantitative label-free imaging of different molecules. The realization of such a powerful combination is obtained through dual-soliton pulses based on a single fiber laser source under the spectral focusing mechanism. All-fiber laser source for CARS application is advantageous over the free space lasers in terms of its simplicity, flexibility and lower cost. Dual-soliton generation just takes advantage of a piece of PM-PCF fiber without any change of laser cavity or extra modulation. The experimental implementation of DS-CARS is straightforward and could be used in less favorable environments while being more compact. All these features are unique to the DS-CARS scheme and differ from previously reported efforts aimed at suppressing the NR background signals in CARS. In addition, advanced

Biomedical Optics EXPRESS

spectral focusing was proposed and established recently by further exploring the potential of this technique [25,26], and we believe that this improvement will benefit the DS-CARS method.

Since the DS-CARS method removes the nonresonant background and measures Raman-like vibrational signals in both microspectroscopy and microscopy, we can perform label-free imaging at multiple characteristic vibrational frequencies to obtain more information about the distributions of multiple chemical species. As we demonstrate in this work, the combination of ratio imaging and in situ background-free microspectroscopy is a powerful tool for study of inhomogeneous samples. The strength of C = C double bond stretching over CH_2 deformation vibrations (I_{1260}/I_{1300} and I_{1450}/I_{1650}) can quantify the degree of lipid-chain unsaturation in the fatty acids mixture, benefiting the reveal of the function of lipid droplets in health and disease. Besides, multiplex DS-CARS imaging is further identified to quantify different oil droplets by the peak intensity ratio. This distinct vibrational markers (I_{1260}/I_{1300} and I_{1450}/I_{1650}) can be used to quantitatively map the spatial variations in the level of lipid unsaturation and acyl-chain order of different lipid droplets within a single cell, or even within individual lipid droplets. Although the DS-CARS capability has been demonstrated by use of a spectrometer with a CCD, it is a parallel process and significantly limit the imaging speed. However, enlarging the temporal interval between the dual-soliton pulses by a longer PCF can allow the utilization of a single detector, such as APD or PMT to accelerate the imaging speed. Besides, our method allows intrinsically feasible tunability of excitation for CARS based on the dual-soliton supercontinuum generation, and we can obtain fingerprint vibrational spectroscopy and images over a large spectral range (800-2200 cm^{-1}) with a spectral resolution of 15 cm^{-1}. This vibrational region has profound chemical information and can help to explore complicated biochemical processes in cells and tissues.

Acknowledgment

We thank Dr. Tao Chen for the help to acquire spontaneous Raman spectra of samples. This work is supported by the State Key Laboratory of Precision Measurement Technology & Instrument of Tsinghua University and the Tsinghua University Initiative Scientific Research Program.